Analysis of Human Whole-body Joint Torques during Overhead Work with a Passive Exoskeleton

Claudia Latella, Yeshasvi Tirupachuri, Luca Tagliapietra, Lorenzo Rapetti, Benjamin Schirrmeister, Jonas Bornmann, Daša Gorjan, Jernej Čamernik, Pauline Maurice, Lars Fritzsche, et al.

Analysis of Human Whole-body Joint Torques during Overhead Work with a Passive Exoskeleton

Claudia Latella[1], Yeshasvi Tirupachuri[1*], Luca Tagliapietra[1*], Lorenzo Rapetti[1 2], Benjamin Schirrmeister[3*], Jonas Bornmann[3], Daša Gorjan[4*], Jernej Čamernik[4*], Pauline Maurice[5], Lars Fritzsche[6], Jose Gonzalez-Vargas[3], Serena Ivaldi[5], Jan Babič[4], Francesco Nori[1*], Daniele Pucci[1]

***Abstract*—Overhead work is classified as one of the major risk factors for the onset of shoulder work-related musculoskeletal disorders (WMSDs) and muscle fatigue. Upper-limb exoskeletons can be used to assist workers during the execution of industrial overhead tasks to prevent such disorders. Twelve novice participants have been equipped with inertial and force/torque sensors to simultaneously estimate the whole-body kinematics and the joint torques (i.e., internal articular stress) by means of a probabilistic estimator while performing an overhead task with a pointing tool. An evaluation has been performed to analyze the effect at the whole-body level by considering the conditions of wearing and not-wearing PAEXO, a passive exoskeleton for upper-limb support during overhead work. Results point out that PAEXO provides a reduction of the whole-body joint effort across the experimental task blocks (from 66% to 86%). Moreover, the analysis along with 5 different body areas shows that i) the exoskeleton provides support at the human shoulders by reducing the joint effort at the targeted limbs and ii) that part of the internal wrenches is intuitively transferred from the upper body to the thighs and legs, which is shown with an increment of the torques at the legs joints. The promising outcomes show that the probabilistic estimation algorithm can be used as a validation metric to quantitatively assess PAEXO performances, paving thus the way for the next challenging milestone, such as the optimization of the human joint torques via adaptive exoskeleton control.**

***Index Terms*—Human whole-body joint torque, floating-base estimation, upper-limb exoskeleton, overhead work analysis**

I. Introduction

Exoskeletons have been part of the robotics scenario for several decades. The scientific interest in exoskeleton-based devices was born in the early '60s to augment human performances for military purposes [1]. Since then, exoskeleton development has evolved into a powerful tool for medical/rehabilitation purposes, where exoskeletons are used to help impaired patients or elderly people to perform daily-life activities [2] [3] [4]. The last decade, however, revealed a rising demand for exoskeletons tailored for industrial applications [5] [6]. For example, assembly-line workers are highly exposed to the genesis of pathologies related to physical stress due to repetitive upper-body movements (e.g., in the automotive workplace, workers have to reach above their heads thousands of times a day when working on the underside of cars). The 2019 report of the European Union on the working conditions in a global perspective [7] showed that pathologies related to repetitive hand or arm movements are the most pervasive job-related risk by affecting more than 60% of the working population in Europe. The report claims that holding a painful body posture (43%) or carrying heavy loads (32%) are other important risk factors for European workers. An industrial exoskeleton can compensate for these drawbacks by providing physical assistance to its user via assistive torques. Industrial exoskeletons have been therefore recently developed to *prevent* work-related musculoskeletal disorders (WMSDs) and not only to *rehabilitate* existing pathologies.

Overhead work has been classified as one of the major risk factors for the onset of shoulder WMSDs and muscle fatigue [8]. Occupational upper-limb exoskeletons can be used to assist workers during the execution of overhead tasks to prevent shoulder WMSDs. Several investigations have been recently conducted on upper-limb exoskeletons showing a reduction of muscle fatigue while executing an overhead task [9] [10] [11]. PAEXO (Ottobock SE & Co. KGaA, Duderstadt, Germany), EksoVest (Ekso Bionics, Richmond, CA, USA), MATE (Comau, Turin, Italy), ShoulderX (SuitX, Emeryville, CA, USA), and SkelEx (Skel-Ex, Rotterdam, The Netherlands) are only some of the relevant commercialized examples of upper-extremity exoskeletons for arm support in overhead work. This category of exoskeletons has been conceived for i) compensating the effect of the gravity on the arm, ii) reducing the upper-body biomechanical loads, iii) preventing long term WMSDs while $iiii$) guaranteeing the work quality and productivity for the companies.

To reduce WMSDs, industrial exoskeletons have also the potential to save substantial costs caused by occupational injuries. It is therefore not surprising that companies are moving towards the large-scale adoption of exoskeletons for their workers for promoting modern production industrial methods. In this respect, in 2018 Ottobock announced the largest long-

[1] Artificial and Mechanical Intelligence at Istituto Italiano di Tecnologia, Center for Robotics Intelligent Systems, Via San Quirico 19D, Genoa, Italy. (email: name.surname@iit.it)

[2] Machine Learning and Optimisation, The University of Manchester, Manchester, United Kingdom

[3] Ottobock SE & Co. KGaA, Max-Näder Str. 15, 37115 Duderstadt, Germany. (email: name.surname@ottobock.de)

[4] Laboratory for Neuromechanics and Biorobotics, Department of Automation, Biocybernetics and Robotics, Jožef Stefan Institute, Jamova cesta 39, SI-1000 Ljubljana, Slovenia. (email: name.surname@ijs.si)

[5] Université de Lorraine, CNRS, Inria, LORIA, F-54000 Nancy, France. (email: name.surname@inria.fr)

[6] imk automotive GmbH, Amselgrund 30, 09128 Chemnitz, Germany. (email: name.surname@imk-automotive.de)

[*] Supplementary email (authorship order): yeshasvitvs@gmail.com , luca.tagliapietra@unipd.it , benjamin.schirrmeister@gmail.com , dasa.gorjan@gmail.com , jernej.camernik@uni-ulm.de , fnori@google.com

term pilot test of exoskeletons in Europe and successfully rolled out in Volkswagen plants several PAEXOs, their passive upper-limb exoskeleton. The pilot test has been carried out to mimic real assembly-line overhead working conditions with 30 employees. The test found a remarkable success among the workers whose subjective feedbacks were very positive [12]. This reason has been the engine for the quantitative assessment analysis carried out in the *in-lab* study in [13] where effects of the PAEXO have been evaluated with respect to (w.r.t.) objective and subjective criteria. Results showed that the exoskeleton reduces shoulder physical strain as well as global physiological strain. However, the study did not analyze the effects of PAEXO at the whole-body internal wrenches level, which is also a pivotal aspect for a better comprehension of the long-term effects of using the exoskeleton. Therefore, a further step has been done in this paper to strengthen the results achieved in [13]. It complements the previous work with a quantitative joint torque estimation assessment at the whole-body effort level. The effort analysis has been performed via a floating-base whole-body joint torque estimation algorithm based on a *Maximum-A-Posteriori* (MAP) estimator implementation. The estimation algorithm has been already validated in [14] w.r.t. standard inverse dynamics methods. The main MAP advantage concerns the possibility to discriminate between sensors according to their reliability (in terms of sensor covariance tuning). Furthermore, the MAP has been developed in such a way to be integrated into a real-time software architecture for the simultaneous estimation of kinematics and dynamics for robotics-based applications.

The novelty proposed in this paper is twofold. On one hand, we exploit the scalability of the estimation algorithm by introducing the exoskeleton as a wearable device, i.e., a *new* type of sensor in the network. On the other hand, we define a *new* metric to evaluate the whole-body support provided by the exoskeleton. The definition of the new approach implicitly embodies a benefit when compared to standard experimental assessments of the human effort. From an experimental perspective, for example, it's impractical to distribute EMGs all over the body to gather the whole-body biomechanical effects.

The paper is structured as follows. Section II defines the mathematical notation and the human kinematics and dynamics modeling. It also recalls the PAEXO description. Furthermore, the algorithm formulation for computing the joint torque estimation is here discussed. In Section III the set-up and the instrumentation for the overhead experiment are described. Section IV discusses the algorithmic approach for the joint torque estimation analysis. Section V presents analysis results. Discussion on the results and several conclusions are reported in Section VI and VII, respectively.

II. Background

A. Notation

- Let $\boldsymbol{x} \in \mathbb{R}^n$ denote a n-dimensional column vector when written in bold text; a scalar quantity when written in non-bold text (i.e., x).
- Let $\mathcal{I}$ be an inertial frame with z axis pointing against the gravity (g denotes the norm of the gravitational acceleration). $\mathcal{B}$ denotes the base frame, i.e., a frame attached to the base link of the system.
- Let ${}^{\mathcal{I}}\boldsymbol{o}_{\mathcal{B}} \in \mathbb{R}^3$ be the coordinate vector connecting the origin of $\mathcal{I}$, i.e., $O_{\mathcal{I}}$, with the origin of $\mathcal{B}$, i.e., $O_{\mathcal{B}}$, pointing towards $O_{\mathcal{B}}$, and expressed w.r.t. $\mathcal{I}$.
- Let $\mathcal{C}[\mathcal{I}]$ be the centroidal frame, i.e., a frame with the origin in the center of mass (COM) and the orientation of the inertial frame $\mathcal{I}$.
- Let ${}^{\mathcal{I}}\boldsymbol{R}_{\mathcal{B}} \in SO(3)$ be a rotation matrix such that ${}^{\mathcal{I}}\boldsymbol{o}_{\mathcal{L}} = {}^{\mathcal{I}}\boldsymbol{o}_{\mathcal{B}} + {}^{\mathcal{I}}\boldsymbol{R}_{\mathcal{B}}\, {}^{\mathcal{B}}\boldsymbol{o}_{\mathcal{L}}$, being $\mathcal{L}$ the frame associated to a link.
- Let $\mathbf{S}(\boldsymbol{x}) \in so(3)$ denote the skew-symmetric matrix $\mathbf{S}(\boldsymbol{x})\boldsymbol{y} = \boldsymbol{x} \times \boldsymbol{y}$, being the cross product operator $\times \in \mathbb{R}^3$.
- Let ${}^{\mathcal{I}}\dot{\boldsymbol{o}}_{\mathcal{B}}$ denote the first-order time derivative of ${}^{\mathcal{I}}\boldsymbol{o}_{\mathcal{B}}$.
- Let $\boldsymbol{f} \in \mathbb{R}^6$ be a 6D wrench vector (3 forces, 3 moments).

B. Recall on system dynamics modeling

The human model is conceived as a rigid multi-body system composed of N_B rigid bodies, called *links*, connected by n joints with one internal Degree of Freedom (DoF) each. We assume that none of the links have a known *a priori* constant pose w.r.t. $\mathcal{I}$. Thus, we say that the system is floating base. The system configuration space is a Lie group $\mathbb{Q} = \mathbb{R}^3 \times SO(3) \times \mathbb{R}^n$, such that $\boldsymbol{q} = (\boldsymbol{q}_b, \boldsymbol{s}) \in \mathbb{Q}$, being the quantity $\boldsymbol{q}_b = ({}^{\mathcal{I}}\boldsymbol{o}_{\mathcal{B}}, {}^{\mathcal{I}}\boldsymbol{R}_{\mathcal{B}}) \in \mathbb{R}^3 \times SO(3)$ the pose of the base frame $\mathcal{B}$ w.r.t. $\mathcal{I}$ and $\boldsymbol{s} \in \mathbb{R}^n$ the joint positions vector capturing the topology of the system. The velocity of the system is represented by $\boldsymbol{\nu} = ({}^{\mathcal{I}}\boldsymbol{v}_{\mathcal{B}}, \dot{\boldsymbol{s}}) \in \mathbb{R}^{6+n}$ where ${}^{\mathcal{I}}\boldsymbol{v}_{\mathcal{B}} = ({}^{\mathcal{I}}\dot{\boldsymbol{o}}_{\mathcal{B}}, {}^{\mathcal{I}}\boldsymbol{\omega}_{\mathcal{B}}) \in \mathbb{R}^6$ is the velocity of $\mathcal{B}$ w.r.t. $\mathcal{I}$ (with ${}^{\mathcal{I}}\boldsymbol{\omega}_{\mathcal{B}}$ angular velocity of the base such that ${}^{\mathcal{I}}\dot{\boldsymbol{R}}_{\mathcal{B}} = \mathbf{S}({}^{\mathcal{I}}\boldsymbol{\omega}_{\mathcal{B}}){}^{\mathcal{I}}\boldsymbol{R}_{\mathcal{B}}$), and $\dot{\boldsymbol{s}} \in \mathbb{R}^n$ the joint velocities vector. If the system is interacting with the external environment by exchanging n_c wrenches, the dynamics of the floating-base system can be described by adopting the Euler-Poincaré formalism [15], (Ch. 13.5):

$$\boldsymbol{M}(\boldsymbol{q})\dot{\boldsymbol{\nu}} + \boldsymbol{h}(\boldsymbol{q}, \boldsymbol{\nu}) = \boldsymbol{B}\boldsymbol{\tau} + \sum_{k=1}^{n_c} \mathbf{J}_{\mathcal{C}_k}^{\top}(\boldsymbol{q})\boldsymbol{f}_k^{ext} \ , \tag{1}$$

where, $\boldsymbol{M} \in \mathbb{R}^{(n+6)\times(n+6)}$ is the mass matrix, $\boldsymbol{h} \in \mathbb{R}^{n+6}$ a vector accounting for the centrifugal and Coriolis effects and gravity terms, $\boldsymbol{B} := (\mathbf{0}_{n\times 6}, \mathbf{1}_n)^{\top}$ is a selector matrix for the joint torque vector $\boldsymbol{\tau} \in \mathbb{R}^n$. $\boldsymbol{f}_k^{ext} \in \mathbb{R}^6$ is a vector representing the external wrench acting on the link that has the k-th contact point. The Jacobian $\mathbf{J}_{\mathcal{C}_k}(\boldsymbol{q}) \in \mathbb{R}^{6\times(6+n)}$ is an operator mapping the system velocity $\boldsymbol{\nu}$ with the velocity $\boldsymbol{v}$ of the k-th contact frame $\mathcal{C}_k$, such that

$${}^{\mathcal{I}}\boldsymbol{v}_{\mathcal{C}_k} = \mathbf{J}_{\mathcal{C}_k}(\boldsymbol{q})\boldsymbol{\nu} = \begin{bmatrix}\mathbf{J}_b(\boldsymbol{q}) & \mathbf{J}_s(\boldsymbol{q})\end{bmatrix} \begin{bmatrix}{}^{\mathcal{I}}\boldsymbol{v}_{\mathcal{B}} \\ \dot{\boldsymbol{s}}\end{bmatrix} \ , \tag{2}$$

where, $\mathbf{J}_b(\boldsymbol{q}) \in \mathbb{R}^{6\times 6}$ and $\mathbf{J}_s(\boldsymbol{q}) \in \mathbb{R}^{6\times n}$ are the Jacobians related to the base and joint configuration, respectively.

Furthermore, it is assumed that a set of holonomic constraints act on the system in Eq. (1) . These constraints may represent, for instance, a frame having a constant pose w.r.t. $\mathcal{I}$. If this frame corresponds to $\mathcal{C}_k$, then ${}^{\mathcal{I}}\boldsymbol{v}_{\mathcal{C}_k} = \mathbf{0}$. Thus, we represent the holonomic constraint such as

$$\mathbf{0} = \mathbf{J}_{\mathcal{C}_k}(\boldsymbol{q})\boldsymbol{\nu} \ . \tag{3}$$

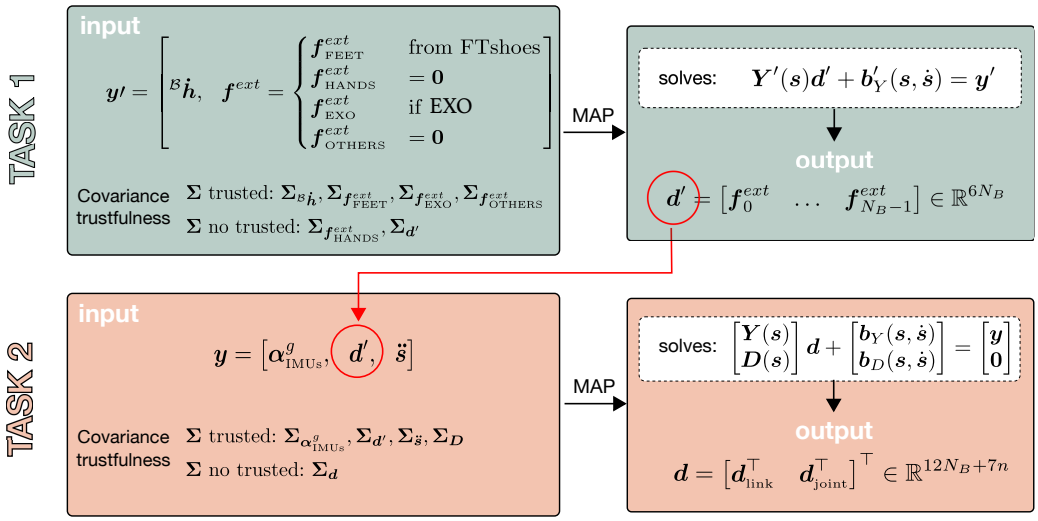

Fig. 1: *Maximum-A-Posteriori* (MAP) algorithm with the Stack-of-Tasks (SoT) variant. The whole estimation algorithm is treated as a stack of two tasks (Task 1 and Task 2) as described in Section II-D.

The first-order time derivative of Eq. (3) yields to

$$\mathbf{0} = \dot{\mathbf{J}}_{\mathcal{C}_k}(\boldsymbol{q})\boldsymbol{\nu} + \mathbf{J}_{\mathcal{C}_k}(\boldsymbol{q})\dot{\boldsymbol{\nu}} \ . \tag{4}$$

Equations (1) and (4) represent the constrained dynamics of a floating-base system.

C. The floating-base whole-body joint torque estimation

The floating-base estimation of the whole-body joint torques has been performed via a probabilistic approach by means of a Stack-of-Tasks *Maximum-A-Posteriori* (SoT MAP) estimator. To this purpose, Eq. (1) and (4) have been equivalently rearranged into a compact matrix form, i.e.,

$$\begin{bmatrix} \boldsymbol{Y}(\boldsymbol{s}) \\ \boldsymbol{D}(\boldsymbol{s}) \end{bmatrix} \boldsymbol{d} + \begin{bmatrix} \boldsymbol{b}_Y(\boldsymbol{s}, \dot{\boldsymbol{s}}) \\ \boldsymbol{b}_D(\boldsymbol{s}, \dot{\boldsymbol{s}}) \end{bmatrix} = \begin{bmatrix} \boldsymbol{y} \\ \mathbf{0} \end{bmatrix} \ , \tag{5}$$

where, $\boldsymbol{Y}$ is a matrix accounting for the sensor measurements, $\boldsymbol{D}$ is a matrix for the system constraints. Bias terms $\boldsymbol{b}_Y$ and $\boldsymbol{b}_D$ are related to the above-listed matrices, respectively. The vector $\boldsymbol{y}$ contains the measurements injected into the algorithm, such as IMUs and force/torque sensors. The vector $\boldsymbol{d}$ embodies kinematics and dynamics quantities for links and joints of the model, i.e.,

$$\boldsymbol{d} \ = \ \left[\boldsymbol{d}^\top_{\text{link}} \quad \boldsymbol{d}^\top_{\text{joint}} \right]^\top \in \mathbb{R}^{12N_B+7n} \ , \tag{6}$$

where,

$$\boldsymbol{d}_{\text{link}} = \left[\boldsymbol{\alpha}^g_0 \quad \boldsymbol{f}^{ext}_0 \quad \dots \quad \boldsymbol{\alpha}^g_{N_B-1} \quad \boldsymbol{f}^{ext}_{N_B-1} \right] \in \mathbb{R}^{12N_B} \ , \tag{7a}$$

$$\boldsymbol{d}_{\text{joint}} = \left[\boldsymbol{f}_1 \quad \dots \quad \boldsymbol{f}_n \quad \ddot{s}_1 \quad \dots \quad \ddot{s}_n \right] \in \mathbb{R}^{7n} \ , \tag{7b}$$

being $\boldsymbol{\alpha}^g \in \mathbb{R}^6$ the proper sensor acceleration, $\boldsymbol{f} \in \mathbb{R}^6$ the internal joint wrench and $\ddot{s}$ the joint acceleration. The goal of the algorithm is to solve Eq. (5) in the variable $\boldsymbol{d}$. The vector in Eq. (6) implicitly contains the joint torque τ as a projection of $\boldsymbol{f}$ on the joint motion freedom subspace $\mathbb{S}$, such that $\tau = \mathbb{S}^\top \boldsymbol{f}$, $\forall n$. The algorithm maximizes the probability of $\boldsymbol{d}$ given the measurements availability. In this (Gaussian) domain, both the vectors $\boldsymbol{d}$ and $\boldsymbol{y}$ are stochastic variables. The estimator, therefore, looks for the mean of a conditional probability, i.e., $\boldsymbol{d} = \boldsymbol{\mu}_{d|y}$, and its covariance $\boldsymbol{\Sigma}_{d|y}$, such as

$$\left[\boldsymbol{\mu}_{d|y}, \boldsymbol{\Sigma}_{d|y} \right] = \arg\max_{\boldsymbol{d}} p(\boldsymbol{d}|\boldsymbol{y}) \ . \tag{8}$$

In Fig. 1, the choice of the covariances $\boldsymbol{\Sigma}$ plays a pivotal role. Covariances accounts for the reliability of i) the sensors input quantities (i.e., $\boldsymbol{\Sigma}_{\boldsymbol{\alpha}}$ from IMUs and $\boldsymbol{\Sigma}_{\boldsymbol{f}^{ext}}$ from force/torque sensors and exoskeleton), ii) the model constraints (i.e., $\boldsymbol{\Sigma}_{\boldsymbol{D}}$) and iii) the prior knowledge on the solution (i.e., $\boldsymbol{\Sigma}_{\boldsymbol{d}}$). Trusted covariances are typically low values. Conversely, high values stand for non-trusted covariances. Technical details for building the system in Eq. (5) and the formulation of its solution in Eq. (8) can be found in [14].

D. The Stack-of-Task (SoT) variant

The SoT MAP variant [16] allows to solve the algorithm by decoupling the estimation of the joint torques from the internal wrench estimation. An important advantage of using the SoT variant is the possibility to estimate those non-collocated wrenches for which physical sensors for the measurements are not available, e.g., external wrenches at the hands without having sensorized gloves placed on them. From an implementation perspective, the variant solves system in Eq. (5) as a stack of two tasks, as described in the pipeline of Fig. 1.

1) Task 1: computation of the equation

$$\boldsymbol{Y}'(\boldsymbol{s})\boldsymbol{d}' + \boldsymbol{b}'_Y(\boldsymbol{s}, \dot{\boldsymbol{s}}) = \boldsymbol{y}' \ , \tag{9}$$

where, $\boldsymbol{y}'$ is a vector containing only a subset of $\boldsymbol{y}$ measurements. The subset encompasses whole-body external wrenches $\boldsymbol{f}^{ext}$ and a new constraint on the rate of change of the centroidal momentum ${}^{\mathcal{B}}\dot{\boldsymbol{h}}$ expressed w.r.t. the base frame $\mathcal{B}$ as follows:

$${}^{\mathcal{B}}\dot{\boldsymbol{h}} = {}^{\mathcal{B}}\boldsymbol{X}^*_{\mathcal{C}[\mathcal{I}]} \begin{bmatrix} m\ {}^{\mathcal{C}[\mathcal{I}]}\ddot{\boldsymbol{x}}_{\text{COM}} \\ \mathbf{0}_{3\times 1} \end{bmatrix} = {}^{\mathcal{B}}\boldsymbol{X}^*_{\mathcal{C}[\mathcal{I}]} \sum_{i=1}^{N_B} \boldsymbol{f}^{ext}_i \ , \tag{10}$$

where, ${}^{\mathcal{B}}\boldsymbol{X}^*_{\mathcal{C}[\mathcal{I}]}$ is the 6×6 adjoint transform for the external wrenches expressed w.r.t. the centroidal frame $\mathcal{C}[\mathcal{I}]$ into the

Fig. 2: Ottobock PAEXO assistive passive exoskeleton.

base frame $\mathcal{B}$. Term m denotes the mass of the model, $\ddot{\boldsymbol{x}}_{\text{COM}}$ is the acceleration of the model COM. The Task 1 solution $\boldsymbol{d}'$ is a vector containing only the estimation of the whole-body external wrenches.

2) Task 2: computation of Eq. (5) by considering the Task 1 output $\boldsymbol{d}'$ as an new input measurement for the Task 2. The measurements vector $\boldsymbol{y}$ encompasses now the entire set of sensor measurements (i.e., the external wrench from the Task 1 estimation and input measurements to $\boldsymbol{y}$ in Task 2).

E. The passive exoskeleton PAEXO

PAEXO is a lightweight passive upper-limb exoskeleton developed by Ottobock SE & Co. KGaA together with Volkswagen AG [17]. PAEXO has been designed to maximize users' freedom of movement and comfort while providing a reasonable assistance. PAEXO provides a support to the user's arms by transferring a portion of the arm weight to a hip belt. It has been designed to i) generate support torques to the users' shoulders, ii) compensate for the arm weight while not hindering or perturbing the motion. Therefore, the provided support varies with the shoulder flexion and arm elevation angle β. It is maximum at $\beta \simeq 90°$ (i.e., upper arm horizontal) and zero when the arm is lowered along the body. The assistive structure of the exoskeleton consists of a support bar and an arm bar connected with a hinge joint (Fig. 2). A passive actuator generates the adjustable support torque in this joint. The structure is attached to the human upper arm with bracelets and to the hip via a hip belt. The exoskeleton is adjustable to fit different body sizes. A textile stabilization structure keeps the support structure close to the body and allows it to move comparable to the shoulder blade. The result is a free movement of the trunk and upper extremities with a weight of only 1.8 kg. Furthermore, the absence of rigid elements in the back enables the full range of back movements. In addition, the level of support can be manually step-less tuned via a mechanical parameter of the passive actuator (i.e., the lever arm length) to adapt to different arm weights or compensate for the extra weight of a tool.

F. The human model

The human body model consists of $N_B = 49$ links and $n = 48$ internal DoFs. The links have been modeled with simple geometric shapes (parallelepiped, cylinder, sphere) whose dimensions are computed via IMU sensors estimation. This approach guarantees the model scalability with the human kinematics. The dynamic properties of each link (i.e., inertias and COM) have been computed using anthropometric data

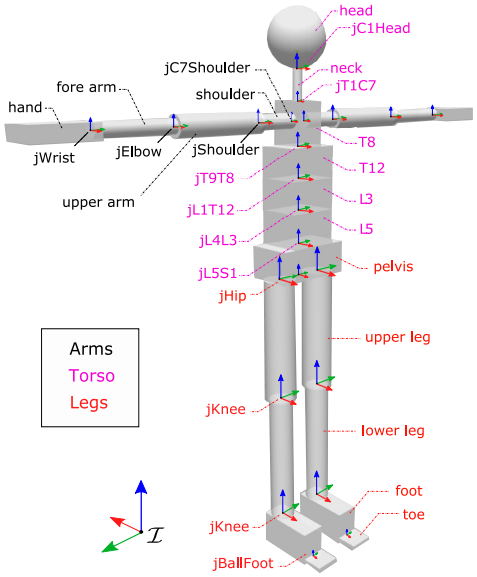

Fig. 3: URDF human whole-body model with links and joints. Labels are classified by body area (black for arms, magenta for torso, red for legs). Red-Green-Blue (RGB) convention is used for x-y-z axes.

available in literature by i) exploiting the relation between the total body mass and the mass of each link [18] and ii) assuming geometric approximations and homogeneous density for the links [19]. A URDF (Universal Robot Description Format) model has been created for representing the kinematics and dynamics of the human multi-body systems [20], Fig. 3. The exoskeleton was not considered in the URDF model but modeled as a set of external wrenches acting on the contact upper-body links (i.e., upper arms, pelvis).

III. The Overhead Experiment

A lab study has been conducted to analyze the effects of PAEXO at the whole-body internal wrenches level. Participants performed a repetitive overhead pointing task, which mimics the tasks commonly observed at the assembly line in the automotive industry. The study was approved by the Slovenian National Medical Ethics Committee (No. 339/2017/7) and it has been conducted in accordance to the Declaration of Helsinki. Data collection is available on-line: https://zenodo.org/record/1472214.

Twelve healthy volunteered males were recruited for the experiment (age: 23.2 ± 1.2 yrs, height: 179.3 ± 5.9 cm, mass: 72.7 ± 5.4 kg). Participants were college students with no or limited industrial experience and novice with exoskeletons. They gave written informed consent before starting the experiment. Participants were told to keep i) their left hand on the frame of an interactive screen horizontally positioned above their head, ii) their feet on two signs placed on the floor below the screen and iii) to perform a task with a hand-held tool (power drill, weight: 0.66 kg) with their right hand, Fig. 4. The task consisted of moving the pointing tool as fast as possible from a starting point to a target, and remaining on the target for 2 s. The screen height was adjusted for each participant so that the tool tip touched the screen when the participant was standing with the right shoulder and elbow

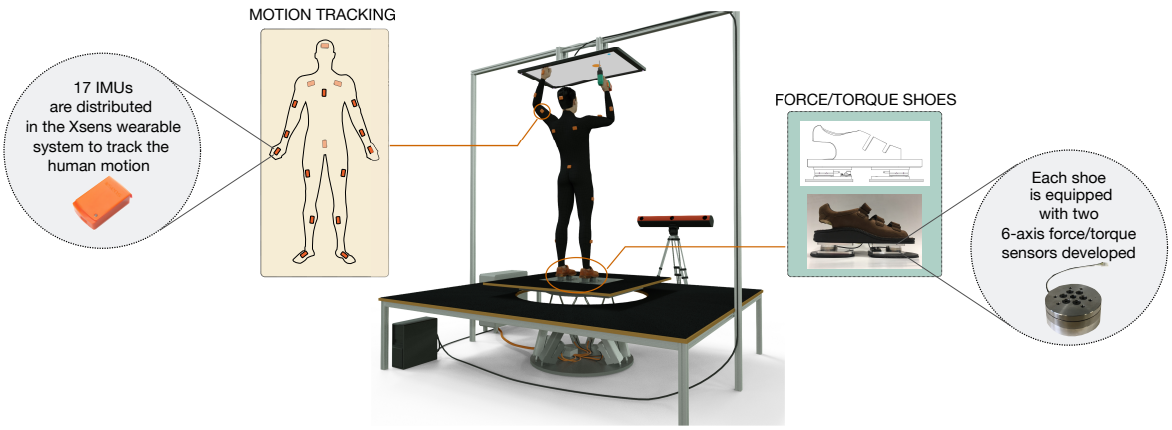

Fig. 4: Schematic view of the experimental set-up with sensors used for the overhead task.

flexed at 90°. The task target was always localized in the center of the screen and appeared in two different sizes: 23 mm and 46 mm diameter. The starting point appeared in 4 different points equally spaced on a circle of radius 1/6th of the participant's height and centered on the target. The target turned green if hit and red if missed. If the target was missed, participants could adjust the tool position until they hit the target. Participants performed the task with the exoskeleton (WE session) and without the exoskeleton (NE session). They were equally divided into 2 groups: A and B. Group A started in NE session and then WE session, while Group B did the opposite to counterbalance the effects of learning and fatigue. Each session consisted of 5 blocks of 24 pointing movements with a 30 s break between blocks. Each block lasted approximately 2 min, resulting in a 12 min long session. Within a block, each combination of target size (2 sizes) and starting position (4 positions) appeared 3 times in random order. Between the two sessions, participants rested for 15 min to prevent experiment-induced fatigue.

A. Instrumentation of the human

Participants were equipped with the Xsens inertial motion tracking wearable system (Xsens, Enschede, The Netherlands) with 17 IMUs to track the whole-body kinematics. Data were recorded with the Xsens MVN software at 60 Hz. A pair of sensorized shoes developed at IIT equipped with four 6-axis force/torque sensors has been used to detect the ground reaction 6D wrenches (3 forces, 3 moments) [21]. Data were recorded at 1 kHz with a custom-made MATLAB script running on Simulink Real-Time.

IV. Joint Torque Estimation Analysis

The whole-body torque analysis has been performed by using the SoT MAP probabilistic estimator described in Fig. 1 for both the NE and WE. The difference between the two sessions concern the inputs in the measurement vector $\boldsymbol{y}$, i.e.,

$$\begin{cases} \boldsymbol{y} = \begin{bmatrix} \boldsymbol{\alpha}^{g}_{\text{IMUs}} & \boldsymbol{f}^{ext}_{\text{SHOES}} \end{bmatrix}^{\top} & \text{if NE} \quad (11) \\ \boldsymbol{y} = \begin{bmatrix} \boldsymbol{\alpha}^{g}_{\text{IMUs}} & \boldsymbol{f}^{ext}_{\text{SHOES}} & \boldsymbol{f}^{ext}_{\text{EXO}} \end{bmatrix}^{\top} & \text{if WE} \quad (12) \end{cases}$$

where, $\boldsymbol{\alpha}^{g}_{\text{IMUs}} \in \mathbb{R}^6$ is the IMUs proper sensor acceleration, $\boldsymbol{f}^{ext}_{\text{SHOES}} \in \mathbb{R}^6$ the sensorized shoes external wrench and $\boldsymbol{f}^{ext}_{\text{EXO}} \in \mathbb{R}^6$ the external force due to presence of the exoskeleton.

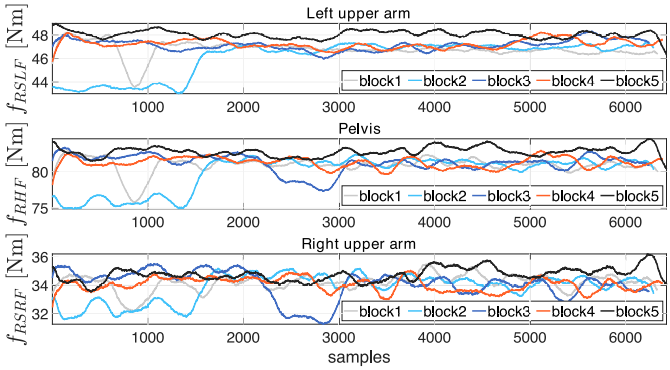

Fig. 5: Inter-subject PAEXO raw force measurements at left arm ($\mathbb{F}_{RSLF}$), hip ($\mathbb{F}_{RHF}$) and right arm ($\mathbb{F}_{RSRF}$), respectively, across 5 blocks.

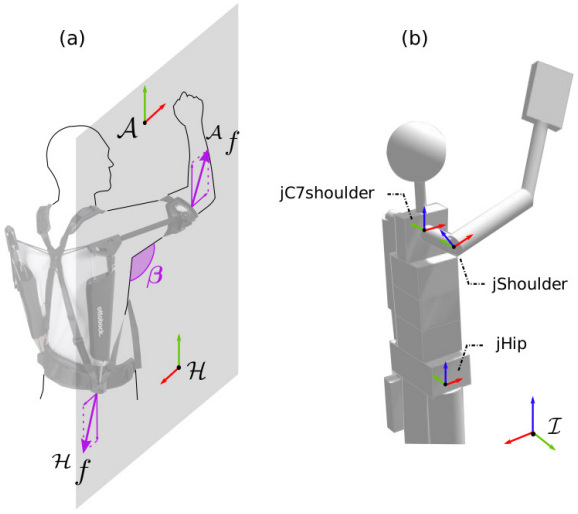

Fig. 6: (a) PAEXO modeling with raw forces at the upper arm (${}^{\mathcal{A}}\mathbb{F}_{RSRF}$) and the hip (${}^{\mathcal{H}}\mathbb{F}_{RHF}$), expressed as a function over the plane of PAEXO elevation arm β. (b) Human URDF modeling with reference frames of the relevant joints for the overhead work. Red-Green-Blue (RGB) convention is used for x-y-z axes.

PAEXO raw measurements $\mathbb{F}_R$ consist of

- a support force for right upper arm, $\mathbb{F}_{RSRF}$,
- a support force for left upper arm, $\mathbb{F}_{RSLF}$,
- a force that is transferred to the hip, $\mathbb{F}_{RHF}$.

Figure 5 shows the raw PAEXO forces measurements $\mathbb{F}_{RSLF}$, $\mathbb{F}_{RHF}$, $\mathbb{F}_{RSRF}$ across 5 blocks, respectively, at the inter-subject level (i.e., on the whole 12-subject dataset). The subjects' posture for block 5 requires a PAEXO maximum support at the arms and this corresponds to an increase of transferred forces at the pelvis. Per each subject, the exoskeleton manufacturer provided raw force measurements computed as a function over the plane of the PAEXO arm elevation angle β (Fig. 6a), in a tabulated format.

A. PAEXO vs. URDF angles compatibility

The first analysis objective required to make the PAEXO angle measurements compatible with the human URDF model defined as in Section II-F. In the URDF model (Fig. 6b), let $\boldsymbol{u} := [u_x \quad u_y \quad u_z]^\top$ be a Euler angle vector which parametrizes a rotation matrix $\boldsymbol{R}$ of the upper arm w.r.t. the shoulder, defined by

$$\boldsymbol{R} := \boldsymbol{R}_x(u_x)\ \boldsymbol{R}_y(u_y)\ \boldsymbol{R}_z(u_z)\ . \tag{13}$$

None of the angles in $\boldsymbol{u}$ coincides with β. Thus, we defined a new Euler angle vector $\boldsymbol{u}' = [u'_x \quad u'_y \quad u'_z]^\top$ to parametrize

$$\boldsymbol{R}' := \boldsymbol{R}_z(u'_z)\ \boldsymbol{R}_x(u'_x)\ \boldsymbol{R}_y(u'_y)\ , \tag{14}$$

that, by construction, is equivalent to Eq. (13) . More in detail, Eq. (14) can be written as

$$\begin{aligned}\boldsymbol{R}' &= \begin{bmatrix} r'_{11} & r'_{12} & r'_{13} \\ r'_{21} & r'_{22} & r'_{23} \\ r'_{31} & r'_{32} & r'_{33} \end{bmatrix} \\ &= \begin{bmatrix} c_{u'_y}c_{u'_z} - s_{u'_x}s_{u'_y}s_{u'_z} & -s_{u'_z}c_{u'_x} & s_{u'_y}c_{u'_z} + s_{u'_x}c_{u'_y}s_{u'_z} \\ s_{u'_z}c_{u'_y} + s_{u'_x}s_{u'_y}c_{u'_z} & c_{u'_x}c_{u'_z} & s_{u'_y}s_{u'_z} - s_{u'_x}c_{u'_y}c_{u'_z} \\ -s_{u'_y}c_{u'_x} & s_{u'_x} & c_{u'_x}c_{u'_y} \end{bmatrix},\end{aligned} \tag{15}$$

and the resulting ZXY Euler angle vector $\boldsymbol{u}'$ [22] is such that

$$u'_x = \text{atan2}\left(r'_{32}, \sqrt{(r'_{12})^2 + (r'_{22})^2}\right)\ , \tag{16a}$$

$$u'_y = \text{atan2}(-r'_{31}, r'_{33})\ , \tag{16b}$$

$$u'_z = \text{atan2}(-r'_{12}, r'_{22})\ . \tag{16c}$$

B. PAEXO vs. URDF forces matching

The further objective was to transform the raw exoskeleton forces into a compatible format for the SoT MAP algorithm, i.e., a wrench vector $\in \mathbb{R}^6$ as required in Eq. (12) . To achieve the goal, we first extracted tabulated forces values accordingly to the new computed vector $\boldsymbol{u}'$. Later, we considered a pure forces assumption (i.e., no moments) on the URDF model per each contact frame $\mathcal{C}_k$ where the exoskeleton exerted a force, (i.e., upper arms, hips).

V. Results

Whole-body joint torque estimation of NE and WE sessions have been compared to assess the effect of the exoskeleton at the inter-subject level. An instance of the estimation algorithm in Fig. 1 has been performed per each subject, each session, over time (i.e., across 5 blocks of a session). Algorithm covariances have been chosen by following a covariance tuning metric, i.e., the minimization of the error between measured and estimated quantities with a relative error such that

$$\epsilon_{rel} = \frac{||\text{meas} - \text{estim}||}{||\text{meas}||} \leq 3\% \ . \tag{17}$$

The 3% threshold is the maximum allowed relative error by mainly taking into account the error of IMUs and also the propagation of the error due to the sensor fusion process.

The mean of the inter-subject whole-body (wb) torques $\bar{\tau}$ [Nm] for NE (orange line) and WE (green line) sessions has been performed across 5 blocks, with the following formulas,

$$\bar{\boldsymbol{\tau}}^{wb}_{NE} = \text{mean} \begin{pmatrix} \boldsymbol{\tau}_1 \\ \boldsymbol{\tau}_2 \\ \vdots \\ \boldsymbol{\tau}_{12} \end{pmatrix}^{wb}_{NE}\ , \quad \bar{\boldsymbol{\tau}}^{wb}_{WE} = \text{mean} \begin{pmatrix} \boldsymbol{\tau}_1 \\ \boldsymbol{\tau}_2 \\ \vdots \\ \boldsymbol{\tau}_{12} \end{pmatrix}^{wb}_{WE}\ , \tag{18}$$

being $\boldsymbol{\tau}_1, \cdots, \boldsymbol{\tau}_{12}$ the subjects whole-body torques estimated by the algorithm. Figure 7 shows a whole-body reduction of the overall joint effort module due to the exoskeleton support with the with related percentage in Table I, across 5 blocks. A statistical analysis has been computed for the inter-subject normalized whole-body torque norm $||\boldsymbol{\tau}^{wb}||$ along with the sessions, across 5 blocks. A two-way repeated-measured analysis of variance (ANOVA) has been performed with two within-subject fixed factors (i.e., sessions and blocks). Subjects are entered as a random factor. Figure 8 shows the evolution of the normalized torque norm across the blocks. The ANOVA reveals a significant effect of the "sessions" factor on the torque estimation ($p\text{-}value < 0.01$). Conversely, the blocks do not affect the estimation ($p\text{-}value = 0.0919$) and no statistical evidence has been detected of an interaction effect between the two factors.

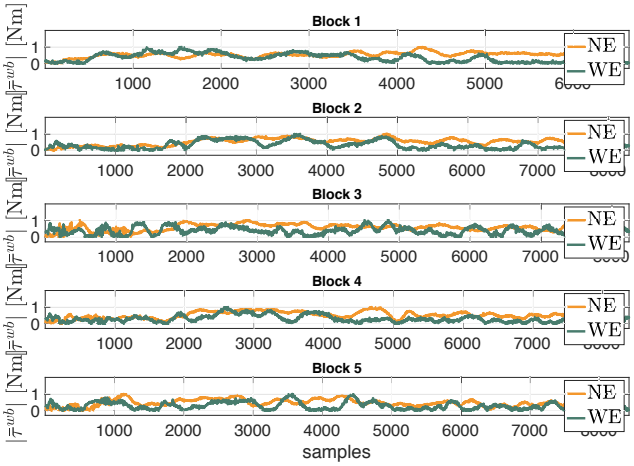

Fig. 7: Normalized inter-subject whole-body mean torques $|\bar{\boldsymbol{\tau}}^{wb}|$ [Nm] for non-exoskeleton (NE) and exoskeleton (WE) sessions, 5 blocks.

	Block 1	Block 2	Block 3	Block 4	Block 5
$\frac{\lvert\bar{\boldsymbol{\tau}}^{wb}_{NE}\rvert - \lvert\bar{\boldsymbol{\tau}}^{wb}_{WE}\rvert}{\lvert\bar{\boldsymbol{\tau}}^{wb}_{NE}\rvert}$	66%	74%	86%	77%	84%

TABLE I: Effort reduction percentage relative to the mean module of the inter-subject whole-body torques $|\bar{\boldsymbol{\tau}}^{wb}|$ of Fig. 7, across 5 blocks.

However, the only whole-body level analysis is not sufficient to assess the effects due to the exoskeleton. An analysis along with 5 different body areas has been performed to evaluate the exoskeleton effects locally to the torso (t), left and right arms (a), left and right legs (l), such as

$$\bar{\bar{\tau}}^{t}_{NE} = \text{mean}(\bar{\boldsymbol{\tau}}^{t}_{NE}) \ , \quad \bar{\bar{\tau}}^{t}_{WE} = \text{mean}(\bar{\boldsymbol{\tau}}^{t}_{WE}) \ , \tag{19a}$$

$$\bar{\bar{\tau}}^{a}_{NE} = \text{mean}(\bar{\boldsymbol{\tau}}^{a}_{NE}) \ , \quad \bar{\bar{\tau}}^{a}_{WE} = \text{mean}(\bar{\boldsymbol{\tau}}^{a}_{WE}) \ , \tag{19b}$$

$$\bar{\bar{\tau}}^{l}_{NE} = \text{mean}(\bar{\boldsymbol{\tau}}^{l}_{NE}) \ , \quad \bar{\bar{\tau}}^{l}_{WE} = \text{mean}(\bar{\boldsymbol{\tau}}^{l}_{WE}) \ . \tag{19c}$$

Figures 9, 10, 11, show the difference between the mean of the inter-subject torques computed for NE and WE for the arms, legs and torso, respectively. Bar plots quantify the magnitude of the effort reduction (green bars) and the effort increase (red bars) in performing the task with the exoskeleton. Plots follow the area division as in Fig. 3. Each cluster of 5 bars (i.e., 5 blocks) represents the entity of the effort reduction/increase for a specific range of motion allowed for the joints (e.g., jL5S1 rot_x represents the rotation around the x axis for the joint jL5S1). The effort due to PAEXO is evident at the arms, especially at both the shoulders (up to $\sim$10 Nm), Fig. 9. Another important evidence is the effort reduction the human gathers on the torso, from L5 to T8 links, Fig. 11. Intuitively, the human gained an effort reduction at the arms and the torso wearing PAEXO at the cost of an increase of the effort at the pelvis and the hips where the load is transferred, Fig. 10.

VI. Discussion

This study analyzed the whole-body effects of the passive upper-limb exoskeleton PAEXO from a joint torque analysis perspective. The analysis has been performed by reproducing in a lab environment the conditions of an industrial overhead work scenario with a dataset of 12 novice participants. A Stack-of-Tasks-based *Maximum-A-Posteriori* (SoT MAP) estimator has been used for the whole-body joint torque estimation of the human modeled as a floating-base system.

A first quantitative analysis in [13] investigated the objective and subjective effects of wearing PAEXO to reduce the WMSDs among overhead workers. This paper complements the previous study by analyzing the effects of PAEXO at the internal wrenches level. From a whole-body promising perspective, the analysis shows that internal whole-body torques are significantly reduced when using the exoskeleton ranging from 66% in Block 1 to a maximum of 86% in Block 3. Moreover, the analysis shows that the presence of the exoskeleton reduces also the internal articular stress at the shoulders and torso level, (Fig. 9, 11). This last outcome is in line with the EMG results of [13] but the analysis offers here a more exhaustive picture of the whole-body biomechanical effects, as well as the unquestioned advantage of an easier doability. However, the reduction of the effort at the upper body is compensated by a general increment of the stress at the legs. Internal wrenches are intuitively transferred to the lower body, especially to the hips (Fig. 10). The right-hand side of Fig. 11 shows a whole-body example of one-subject joint effort visualization. The color of the spheres represents the change in the joint effort for the same task performed in the two sessions, ranging from red (i.e., high effort) to green (i.e., low effort). The time-frame visualization confirms the results just discussed.

VII. Conclusions

The paper achievements show that the estimation algorithm can be used as a validation tool to assess if PAEXO is able to measure quantitatively the overhead workers effort. However, several factors may impact the effectiveness of the results. *From a modeling perspective*, the conceptual design of an exoskeleton requires alignment with the user's biological joint kinematics. The exact position of the human joints axes is impractical to be retrieved *in vivo* thus leading to a mismatch between the device and the real axes. Misalignments (of the order of a couple of centimeters) generate residual wrenches by the propagation of the error. This modifies the physiological kinematics of the body, may increase the physiological demand [23], and often it is perceived by the user as discomfort [24]. This can induce, in turn, an increment of biomechanical stress at a not-targeted limb because of the potential onset of physiological adaptation. Concerning the human-exoskeleton model pairing, the biggest limitation is represented by the difficulty of simulating the body interface at the hip where the exoskeleton is attached. *From an experimental perspective*, experiments have to be carried out with real workers who experience real working issues in an industrial environment. In this regard, the initial laboratory study we presented is a good resource for overcoming possible factories' reluctance to be involved in such trials. In general, the promising outcomes of the analysis pave the way for the very next challenging milestone, such as the optimization of the human joint torques via adaptive exoskeleton control. For the optimization computational cost, it will be extremely useful to use simplified human models rather than musculoskeletal models, thus accepting a loss of accuracy from the biological point of view. This is an acceptable trade-off for the development of control algorithms that can be complemented with musculoskeletal analyses. In general, we envision that in the long run the large-scale adoption of the exoskeleton control will be a fundamental step towards the reduction of WMSDs.

Acknowledgment

This paper is supported by EU An.Dy Project. This project has received funding from the European Union's Horizon 2020 research and innovation programme under grant agreement No. 731540. The content of this publication is the sole responsibility of the authors. The European Commission or its services cannot be held responsible for any use that may be made of the information it contains.

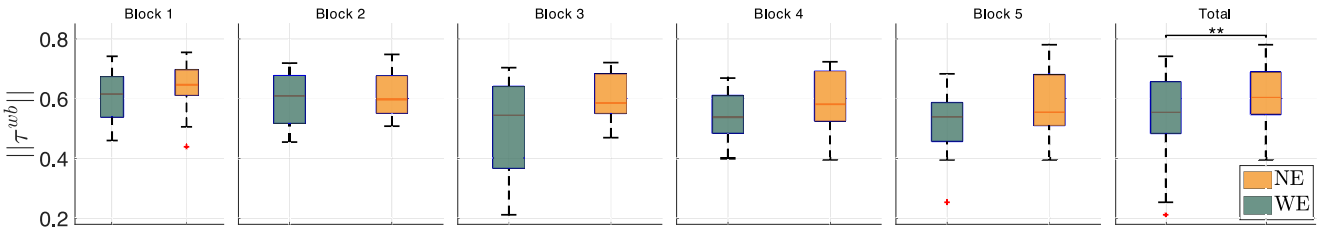

Fig. 8: Comparison of the inter-subject whole-body normalized torque norm $||\boldsymbol{\tau}^{wb}||$ for non-exoskeleton (NE) and exoskeleton (WE) sessions, across 5 blocks. The two-way repeated-measures analysis of variance (ANOVA) shows that the torque estimation is significantly affected by the presence of the exoskeleton while it is not affected by the 5-block division of each session.

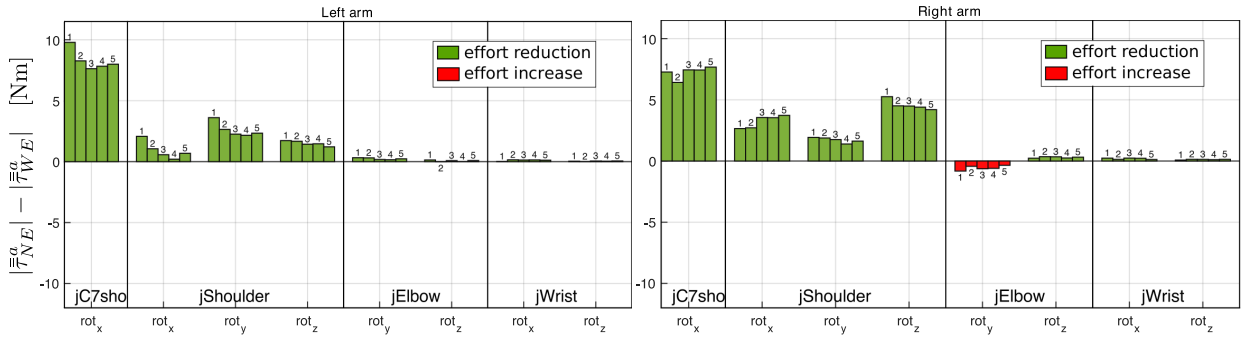

Fig. 9: Difference of the mean of the inter-subject torques $\bar{\bar{\tau}}^a$ [Nm] for non-exoskeleton (NE) and exoskeleton (WE) sessions, across 5 blocks, for the left and right arm, respectively. The torque difference is the metric to investigate the magnitude of the effort reduction (green bars) and the effort increase (red bars) at the arms joints (black labeled in Fig. 3) due to the exoskeleton presence.

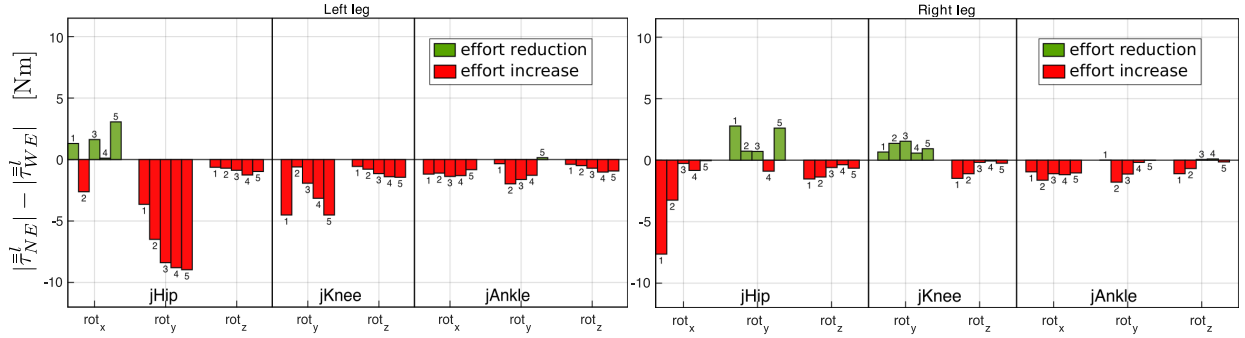

Fig. 10: Difference of the mean of the inter-subject torques $\bar{\bar{\tau}}^l$ [Nm] for non-exoskeleton (NE) and exoskeleton (WE) sessions, across 5 blocks, for the left and right leg, respectively. The torque difference is the metric to investigate the magnitude of the effort reduction (green bars) and the effort increase (red bars) at the legs joints (red labeled in Fig. 3) due to the exoskeleton presence.

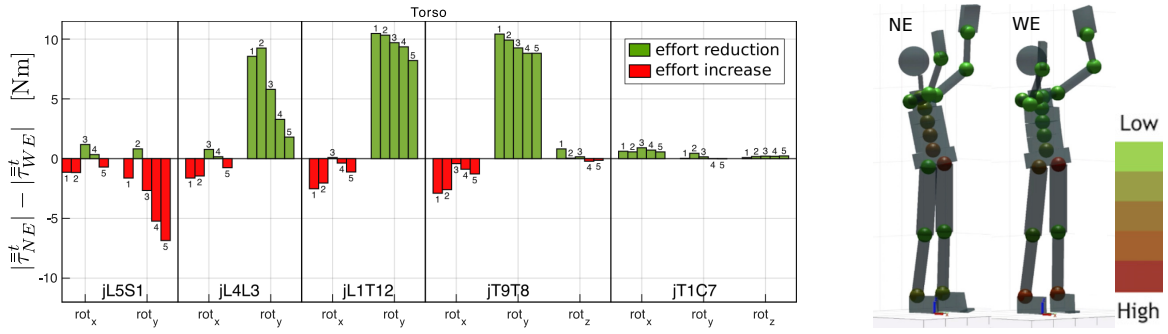

Fig. 11: Difference of the mean of the inter-subject torso torques $\bar{\bar{\tau}}^t$ [Nm] for non-exoskeleton (NE) and exoskeleton (WE) sessions, across 5 blocks. The torque difference is the metric to investigate the magnitude of the effort reduction (green bars) and the effort increase (red bars) at the torso joints (magenta labeled in Fig. 3) due to the exoskeleton presence. On the right-hand side, an example of a one-subject visualization comparison of the joint effort is shown. The color of the spheres represents the change in the joint effort for the same task performed in the two sessions, ranging from red (i.e., high effort) to green (i.e., low effort) .

REFERENCES

[1] N. J. Mizen, "Preliminary design for the shoulders and arms of a powered exoskeletal structure." [Online]. Available: https://apps.dtic.mil/docs/citations/AD0623389

[2] Z. Pineda-Rico, J. A. Sanchez de Lucio, F. J. Martinez Lopez, and P. Cruz, "Design of an exoskeleton for upper limb robot-assisted rehabilitation based on co-simulation." [Online]. Available: https://www.jvejournals.com/article/16857

[3] E. Pirondini, M. Coscia, S. Marcheschi, G. Roas, F. Salsedo, A. Frisoli, M. Bergamasco, and S. Micera, "Evaluation of the effects of the arm light exoskeleton on movement execution and muscle activities: a pilot study on healthy subjects," *Journal of NeuroEngineering and Rehabilitation*, vol. 13, no. 1, p. 9. [Online]. Available: https://doi.org/10.1186/s12984-016-0117-x

[4] Q. Wu, X. Wang, B. Chen, and H. Wu, "Patient-active control of a powered exoskeleton targeting upper limb rehabilitation training," *Frontiers in Neurology*, vol. 9. [Online]. Available: https://www.frontiersin.org/articles/10.3389/fneur.2018.00817/full

[5] M. P. de Looze, T. Bosch, F. Krause, K. S. Stadler, and L. W. O'Sullivan, "Exoskeletons for industrial application and their potential effects on physical work load," *Ergonomics*, vol. 59, no. 5, pp. 671–681.

[6] J. Babič, K. Mombaur, D. Lefeber, J. van Dieën, B. Graimann, M. Russold, N. Šarabon, and H. Houdijk, "SPEXOR: Spinal exoskeletal robot for low back pain prevention and vocational reintegration," in *Wearable Robotics: Challenges and Trends*, ser. Biosystems & Biorobotics, J. González-Vargas, J. Ibáñez, J. L. Contreras-Vidal, H. van der Kooij, and J. L. Pons, Eds. Springer International Publishing, pp. 311–315.

[7] "Eurofound and international labour organization, working conditions in a global perspective, publications office of the european union, luxembourg, and international labour organization, geneva."

[8] J. R. Grieve and C. R. Dickerson, "Overhead work: Identification of evidence-based exposure guidelines," *Occupational Ergonomics*, vol. 8, no. 1, pp. 53–66. [Online]. Available: https://content.iospress.com/articles/occupational-ergonomics/oer00157

[9] K. Huysamen, T. Bosch, M. de Looze, K. S. Stadler, E. Graf, and L. W. O'Sullivan, "Evaluation of a passive exoskeleton for static upper limb activities," *Applied Ergonomics*, vol. 70, pp. 148–155. [Online]. Available: http://www.sciencedirect.com/science/article/pii/S0003687018300334

[10] S. Kim, M. A. Nussbaum, M. I. Mokhlespour Esfahani, M. M. Alemi, S. Alabdulkarim, and E. Rashedi, "Assessing the influence of a passive, upper extremity exoskeletal vest for tasks requiring arm elevation: Part i - "expected" effects on discomfort, shoulder muscle activity, and work task performance," *Applied Ergonomics*, vol. 70, pp. 315–322.

[11] A. Voilqué, J. Masood, J. Fauroux, L. Sabourin, and O. Guezet, "Industrial exoskeleton technology: Classification, structural analysis, and structural complexity indicator," in *2019 Wearable Robotics Association Conference (WearRAcon)*, pp. 13–20.

[12] Volkswagen. When arms learn to fly. [Online]. Available: https://www.volkswagenag.com/en/news/stories/2018/09/when-arms-learn-to-fly.html

[13] P. Maurice, J. Čamernik, D. Gorjan, B. Schirrmeister, J. Bornmann, L. Tagliapietra, C. Latella, D. Pucci, L. Fritzsche, S. Ivaldi, and J. Babič, "Objective and subjective effects of a passive exoskeleton on overhead work," *IEEE Transactions on Neural Systems and Rehabilitation Engineering*, pp. 1–1.

[14] C. Latella, S. Traversaro, D. Ferigo, Y. Tirupachuri, L. Rapetti, F. J. Andrade Chavez, F. Nori, and D. Pucci, "Simultaneous floating-base estimation of human kinematics and joint torques," *Sensors*, vol. 19, no. 12, p. 2794. [Online]. Available: https://www.mdpi.com/1424-8220/19/12/2794

[15] J. E. Marsden and T. Ratiu, *Introduction to Mechanics and Symmetry: A Basic Exposition of Classical Mechanical Systems*, 2nd ed., ser. Texts in Applied Mathematics. Springer-Verlag. [Online]. Available: //www.springer.com/it/book/9780387986432

[16] Y. Tirupachuri, P. Ramadoss, L. Rapetti, C. Latella, K. Darvish, S. Traversaro, and D. Pucci, "Online non-collocated estimation of payload and articular stress for real-time human ergonomy assessment," *IEEE Access*, pp. 1–1. [Online]. Available: https://ieeexplore.ieee.org/document/9526592

[17] J. Bornmann, B. Schirrmeister, T. Parth, and J. Gonzalez-Vargas, "Comprehensive development, implementation and evaluation of industrial exoskeletons," *Current Directions in Biomedical Engineering*, vol. 6, no. 2. [Online]. Available: https://www.degruyter.com/document/doi/10.1515/cdbme-2020-2001/html

[18] D. Winter, *Biomechanics and Motor Control of Human Movement, 4th Edition*. Wiley.

[19] M. R. Yeadon, "The simulation of aerial movement—II. a mathematical inertia model of the human body," *Journal of Biomechanics*, vol. 23, no. 1, pp. 67–74. [Online]. Available: http://www.sciencedirect.com/science/article/pii/002192909090370I

[20] C. Fairchild and T. L. Harman, *ROS Robotics By Example*. Packt Publishing.

[21] I. Sorrentino, F. J. Andrade Chavez, C. Latella, L. Fiorio, S. Traversaro, L. Rapetti, Y. Tirupachuri, N. Guedelha, M. Maggiali, S. Dussoni, G. Metta, and D. Pucci, "A novel sensorised insole for sensing feet pressure distributions," *Sensors*, vol. 20, no. 3, p. 747. [Online]. Available: https://www.mdpi.com/1424-8220/20/3/747

[22] D. Henderson, "Euler angles, quaternions, and transformation matrices working relationships." [Online]. Available: https://ntrs.nasa.gov/citations/19770024290

[23] J. Theurel, K. Desbrosses, T. Roux, and A. Savescu, "Physiological consequences of using an upper limb exoskeleton during manual handling tasks," *Applied Ergonomics*, vol. 67, pp. 211–217.

[24] A. Schiele and F. C. T. v. d. Helm, "Kinematic design to improve ergonomics in human machine interaction," *IEEE Transactions on Neural Systems and Rehabilitation Engineering*, vol. 14, no. 4, pp. 456–469.